Front. Earth Sci. 2018, 12(1): 108–124
https://doi.org/10.1007/s11707-017-0621-8

RESEARCH ARTICLE

Spatiotemporal changes in vegetation net primary productivity in the arid region of Northwest China, 2001 to 2012

Zhen LI, Jinghu PAN (✉)

College of Geographic and Environmental Science, Northwest Normal University, Lanzhou 730070, China

Abstract Net primary productivity (NPP) is recognized as an important index of ecosystem conditions and a key variable of the terrestrial carbon cycle. It also represents the comprehensive effects of climate change and anthropogenic activity on terrestrial vegetation. In this study, the temporal-spatial pattern of NPP for the period 2001–2012 was analyzed using a remote sensing-based carbon model (i.e., the Carnegie-Ames-Stanford Approach, CASA) in addition to other methods, such as linear trend analysis, standard deviation, and the Hurst index. Temporally, NPP showed a significant increasing trend for the arid region of Northwest China (ARNC), with an annual increase of 2.327 g C. Maximum and minimum productivity values appeared in July and December, respectively. Spatially, the NPP was relatively stable in the temperate and warm-temperate desert regions of Northwest China, while temporally, it showed an increasing trend. However, some attention should be given to the northwestern warm-temperate desert region, where there is severe continuous degradation and only a slight improvement trend.

Keywords NPP, CASA model, remote sensing, arid region of Northwest China (ARNC)

1 Introduction

Vegetation net primary productivity (NPP) is defined as the net accumulation of organic matter through photosynthesis by green plants per unit of time and space and represents the net primary source of food energy for Earth's living entities, including human beings (Yu et al., 2009). It is recognized as an important index of ecosystem conditions and is a key variable for the terrestrial carbon cycle. It also represents the comprehensive effects on terrestrial vegetation caused by climate change and anthropogenic activity.

The arid regions of Northwest China (ARNC) are especially susceptible to environmental degradation and desertification (Verstraete, 1986; UN, 1994; Eswaran et al., 2001). Vegetation cover is highly significant in these areas for protection against wind and aeolian erosion (Calvão and Palmeirim, 2004). Therefore, the quantification of biomass and the monitoring of NPP are essential for identifying and monitoring these high risk areas (Moleele et al., 2001; Niklaus et al., 2012), predicting terrestrial carbon cycle trends (Field et al., 1995; Nemani et al., 2003; Yu et al., 2009), determining the sustainable use of natural resources, and making policy decisions (Mu et al., 2013a,c).

It is rather difficult to estimate terrestrial NPP on a large scale by the direct harvest method. Thus, it is necessary to use mathematical models calibrated with existing data to investigate the spatial and temporal variations of NPP (Lin, 2009), some of which include: 1) models that simulate carbon fluxes using a prescribed vegetation structure, e.g., the Biome BioGeochemical Cycles model (BIOME-BGC) (Running et al., 2004) and CENTURY (Parton et al., 1993); 2) models that simulate both vegetation structure and carbon fluxes, e.g., BIOME3 (the third generation Biogenic Model for Emissions) (Haxeltine and Prentice, 1999), DOLY (Woodward et al., 1995) and HYBRID (Esser et al., 1999); and 3) models based on satellite sensors, e.g., the Carnegie Ames Stanford Approach (CASA) (Potter et al., 2004), the Global Production Efficiency Model (GLO-PEM) (Prince and Goward, 1995; Cao et al., 2004), the Simple Diagnostic Biosphere Model (SDBM) (Knorr and Heimann, 1995; Rayner et al., 2005), the Simple Interactive Biosphere Model (SIB2) (Sellers et al., 1996) and the Terrestrial Uptake and Release of Carbon (TURC) model (Ruimy et al., 1996). For example, Running et al. (2004) used the BIOME-BGC model to assess global terrestrial primary production by a

Received March 27, 2016; accepted October 9, 2016

E-mail: panjh-nwnu@163.com

continuous satellite-derived measure. With the development of remote sensing techniques, numerous RS-based models for estimating NPP have been developed in recent decades to study the dynamics of vegetation productivity at scales ranging from local to global. A remote sensing-based carbon model (e.g., the CASA model) uses a light-use efficiency (ε) factor — which is the efficiency of the conversion of light energy into dry materials by plants — to express the effects of air temperature and water stress (Potter et al., 2003). Compared with process-oriented ecosystem models that entail a complex combination of model parameterizations, the CASA model is relatively simpler and more efficient for exploring dynamic changes in NPP and their spatiotemporal variations at larger scales. Moreover, satellite remote sensing provides information about the integrated response of vegetation canopies to environmental factors, including those that might otherwise be neglected in model mechanisms, such as land-use changes, irrigation, and natural hazards (Malmstrom et al., 1997; Hicke et al., 2002a). The CASA model has been successfully implemented by several researchers to simulate NPP over North America, South America, Eurasia, Australia, and Africa at a range of spatial and temporal scales (Field et al., 1995; Hicke et al., 2002b; Piao et al., 2006; Tang et al., 2014). Based on the CASA model, many studies have been conducted to estimate the distribution of terrestrial NPP in mainland China (Fang et al., 2003; Piao et al., 2005; Pei et al., 2013). Chen et al. (2011) investigated the spatial-temporal changes of NPP in China from 1981 to 2008, and Pei et al. (2013) assessed the impacts of drought on NPP in China from 2001 through 2010. Some studies have been carried out at relatively smaller scales, such as in Northeast China, the Tibetan Plateau, and the Heihe River Basin. Others have been performed on single ecological systems, especially grassland, forest, and wetland ecosystems. Comparatively fewer long-term research studies have been carried out in the arid region of Northwest China (ARNC) using the CASA model.

Many ecosystems in the ARNC are deteriorating. We draw attention to the ARNC because it accounts for one quarter of the total land area of China, encompassing a wide range of varied ecosystems and climates, and providing significant potential for biological carbon sequestration or harvesting (Piao et al., 2009). The ARNC also plays a key role in determining the carbon budget at regional scales. Furthermore, the area is characterized as arid or semiarid and poses major ecological challenges due to land degradation and desertification. Extensive changes in land use and land cover have occurred since the late 1970s, leading to large variations in China's terrestrial ecosystem production capacity (Liu et al., 2003; Piao et al., 2010). Therefore, a thorough examination of the spatiotemporal patterns of the ARNC will advance our understanding of regional carbon budgets in a changing environment and will consequently help forecast the potential biosphere feedback to natural and anthropogenic changes in the climate system. In addition, it could predict where and when environmental degradation and desertification will occur in the future.

In this study, we use the CASA model to estimate the terrestrial NPP in the ARNC from 2001 to 2012. Two improvements have been made to the CASA model: 1) the lapse rate and the ordinary Kriging method were combined to simulate temperature, and 2) the sunshine percentage and astronomical radiation were used to fit total solar radiation. In addition, the slope, standard deviation and Hurst methods were used to reveal the spatial and temporal changes of NPP. The slope of the regression method can detect and analyze the temporal tendency of each grid in the long time series. The standard deviation method can reflect the fluctuation. Moreover, the Hurst index can evaluate the persistence or non-persistence of a time series of the NPP. In the end, validations were made to the estimated NPP. The annual mean NPP was first compared to the observations at 40 sites downloaded from the ORNL DAAC (Oak Ridge National Laboratory Distributed Active Archive Center). Results showed that the annual mean NPP was in contrast to the annual Moderate Resolution Imaging Spectroradiometer (MODIS) NPP, with a spatial resolution of 1 km × 1 km using the BIOME-BGC model. Therefore, the main objectives of this study were to: 1) characterize temporal-spatial variations in the ARNC from 2001–2012; 2) improve the CASA model by modifying the climate, vegetation, and plant physio-ecological parameters; 3) explore the temporal and spatial variation of NPP in different natural geographical regions; and 4) provide scientific reference for the restoration and reconstruction of the ecological environment in Northwest China.

2 The study area

The ARNC lies between 70°01′–121°09′E and 36°16′–46°25′N, covering approximately 2.46 million km^2 and is divided based on the natural geographic division of China by Zhao (1983). The Tianshan, Kunlun, Aljin, Qilian, and Great Khingan mountain ranges are successively distributed from west to east (Fig. 1). The climate is typical of inner-continental land masses, with a wide temperature range, low precipitation, and low humidity. It is dominated by continental arid conditions with lesser effects from the East Asian Monsoon (Liu et al., 2010). Precipitation shows an irregular distribution among the different regions. Annual precipitation typically ranges between 100 and 400 mm per year from west to east. The rivers of the ARNC are mostly continental. Runoff from mountainous regions is the primary water resource, and the recharge sources are from rainwater and melt-water. Ecologically, the primary ecosystems in the ARNC are, from east to west, forest steppe, typical steppe, desert steppe, and desert.

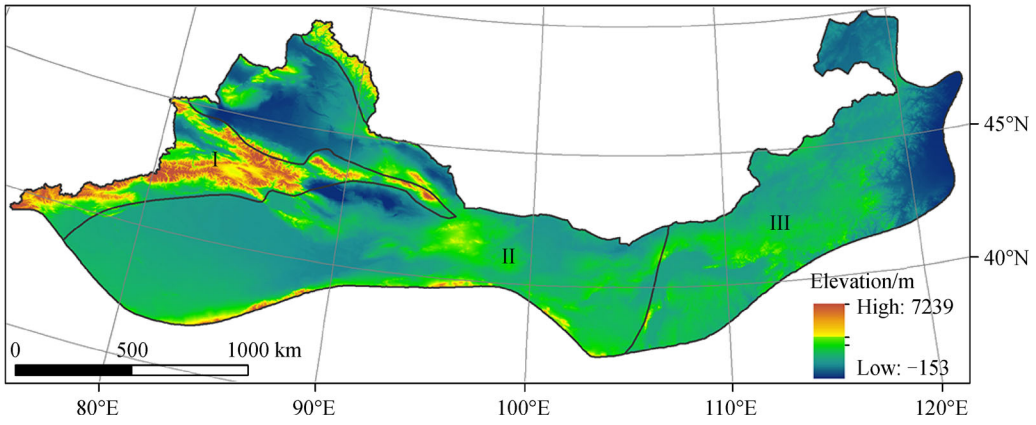

Fig. 1 Comprehensive physical representation of the ARNC. Note: There are three subregions: I, the Xinjiang mountain grassland-coniferous forest region; II, the northwestern warm-temperate desert region; and III, the Inner Mongolia temperate steppe region.

3 Data and methods

3.1 Data

Considering the long east-west extension of the research area, high-resolution satellite data are obviously unsuitable for a large-scale macroscopic study, while low-continuity and low temporal-resolution image processing could introduce errors. The MODIS NDVI (Normalized Difference Vegetation Index) data, however, are continually assessed and validated, providing robust large-scale observations of surface vegetation conditions. MODIS NDVI data with a spatial resolution of 1 km×1 km and a temporal resolution of 16 days, derived from the Atmosphere Archive and Distribution System (LAADS) (http://ladsweb.nascom.nasa.gov/data/order.html) from 2001 to 2012, were used in this study for running the CASA model. These data were re-projected to an Albers equal area projection and WGS84 datum using the MODIS reprojection tool (MRT). Meteorological data, including daily average temperature, daily total precipitation, and daily total radiation for the same period, were obtained from the Chinese Meteorological Data Sharing Service System (http://cdc.cma.gov.cn/home.do). Meteorological data were collected from 314 national meteorological stations and 48 radiation stations built in the ARNC and its surrounding area. In addition, a digital elevation model (DEM) with a grid resolution of 1 km×1 km was supplied by the United States Geological Survey (USGS) and downloaded from the URL http://glovis.usgs.gov/.

3.2 Methods

3.2.1 CASA model

The CASA model is a light-use efficiency-based NPP model, in which NPP is the product of two major driving parameters: absorbed photosynthetically active radiation (APAR, $MJ \cdot m^{-2}$) and light-use efficiency (ε, $g\ C \cdot MJ^{-1}$). The basic principle of the model can be described by the following formula (Yu et al., 2011):

$$NPP(x,t) = APAR(x,t) \times \varepsilon(x,t), \quad (1)$$

where x is the spatial location (the pixel number) and t is the time. $APAR(x, t)$($g\ C \cdot m^{-2} \cdot month^{-1}$) represents the photosynthetically active radiation absorbed by pixel x over time t, while $\varepsilon(x, t)$ represents the actual light-use efficiency ($g\ C \cdot MJ^{-1}$) of pixel x over time t. $APAR(x, t)$ and $\varepsilon(x, t)$ in the model are calculated according to Eqs. (2) to (6) (Wang et al., 2009; Liu et al., 2015):

$$APAR(x,t) = SOL(x,t) \times FPAR(x,t) \times 0.5, \quad (2)$$

$$FPAR(x,t) = \alpha FPAR_{NDVI} + (1-\alpha) FPAR_{SR}, \quad (3)$$

$$FPAR_{NDVI} = \frac{NDVI_{(x,t)} - NDVI_{(i,\min)}}{NDVI_{(i,\max)} - NDVI_{(i,\min)}} \times (FPRA_{\max} - FPRA_{\min}) + FPRA_{\min}, \quad (4)$$

$$FPAR_{SR} = \frac{SR_{(x,t)} - SR_{(i,\min)}}{SR_{(i,\max)} - SR_{(i,\min)}} \times (FPRA_{\max} - FPRA_{\min}) + FPRA_{\min}, \quad (5)$$

$$SR_{(x,t)} = \frac{1 + NDVI_{(x,t)}}{1 - NDVI_{(x,t)}}, \quad (6)$$

where $SOL(x,t)$ is the total solar radiation ($MJ \cdot m^{-2} \cdot month^{-1}$) of pixel x over time t and $FPAR$ is the fraction of photosynthetic active radiation absorbed by the vegetation, which is determined from the satellite-monitored NDVI data. When $FPAR_{\min} = 0.001$ and $FPAR_{\max} = 0.95$, the $NDVI_{(i,\max)}$ value corresponds to 95% of the NDVI production i and the $NDVI_{(i,\min)}$ value corresponds to 5% of the NDVI production i; i is the type

of vegetation. The α value is 0.5, accounting for the fact that approximately half of the incoming solar radiation lies in the photosynthetically active radiation waveband (0.4–0.7 μm) (Potter et al., 1993).

$$\varepsilon(x,t) = T_{\varepsilon 1}(x,t) \times T_{\varepsilon 2}(x,t) \times W_{\varepsilon}(x,t) \times \varepsilon_{\max}, \quad (7)$$

$$T_{\varepsilon 1}(x,t) = 0.8 + 0.02 \times T_{opt}(x) - 0.0005 \times [T_{opt}(x)]^2, \quad (8)$$

$$T_{\varepsilon 2}(x,t) = 1.184/\{1 + \exp[0.2 \times (T_{opt}(x) - 10 - T(x,t))]\} \times 1/\{1 + \exp[0.3 \times (-T_{opt}(x) - 10 + T(x,t))]\}, \quad (9)$$

$$W_{\varepsilon}(x,t) = 0.5 + 0.5 \times E(x,t)/E_p(x,t), \quad (10)$$

where $T_{\varepsilon 1}(x,t)$ and $T_{\varepsilon 2}(x,t)$ are temperature stress coefficients that reflect the reduction of light-use efficiency caused by the temperature factor. $W_{\varepsilon}(x,t)$ is the moisture stress coefficient and indicates the reduction of light-use efficiency caused by the moisture factor. $T_{opt}(x)$ is the mean temperature (°C) during the month of maximum NDVI. $T(x,t)$ is the mean monthly temperature. $E(x,t)$ and $E_p(x,t)$ represent the estimated and potential evapotranspiration and are usually determined from the one-layer budget SMM (Piao et al., 2005; Potter et al., 1993). $\varepsilon_{\max}$ is the maximum light-use efficiency under ideal conditions. The initial value of $\varepsilon_{\max}$ was 0.389 g C·MJ^{-1} according to Potter et al. (1993) in the CASA model, but this value can be significantly affected by a range of environmental factors, such as temperature, water availability, soil type, plant nutrition, disease, individual development, genetic differences, and energy distribution within the ecosystem (Prince, 1991). The present study therefore applied the $\varepsilon_{\max}$ values for different vegetation types, as recommended by Running et al. (2000), by using an eco-physiological model BIOME-BGC. The $\varepsilon_{\max}$ of each vegetation type is different. The $\varepsilon_{\max}$ values for the needle-leaf forest, broadleaf forest, bush, grassland, and farmland were set to 1.008 g C·MJ^{-1}, 1.044 g C·MJ^{-1}, 0.768 g C·MJ^{-1}, 0.608 g C·MJ^{-1}, and 0.604 g C·MJ^{-1}, respectively (Running et al., (2000)). The values of $\varepsilon_{\max}$ for the barren, sparsely vegetated types and other ecosystems in this study were defined to be the same as the constant value in the original CASA model (0.389 g C·MJ^{-1}). More details about the CASA model, including descriptions of the calibration and data processing, can be found in Yu et al. (2011) and Wang et al. (2009). Figure 2 is a flow chart of the CASA algorithm used to simulate the NPP.

3.2.2 Simulating the spatial distribution of temperature data

The monthly average temperature changes over altitude. Under certain conditions, such as at high altitude, there are significant differences in the spatial distribution of temperature. Usually, within the scope of the troposphere, the temperature decreases with a rise in altitude, and for every 100 m rise above sea level, the average temperature drops 0.65°C. However, the vertical lapse rate will vary with the seasons (Li et al., 2006). According to the monthly average temperature data from the 314 high-elevation weather stations utilized in this study, Eq. (11) can be used to calculate the average temperature of the nation's vertical decline rate.

$$T_i = a_t \times H + b_i, \quad (11)$$

where T_i is the monthly average temperature (°C); a_t is a regression coefficient; b_i is the residual error; H is the altitude (m); and i is the ordinal number of the month (from 1 to 12). Based on the vertical decline rate and meteorological site elevations, the observed temperature for elevation "0" correlates well with the simulated temperature of elevation "0" ($T_{k(x,t)}$) using the Ordinary Kriging spatial interpolation method. This method is based on variation functions theory and structure analysis (see Table 1). It uses the original data of regionalized variables and the structural characteristics of variation functions. It also adopts the weighted average of variable values of observation points to ascertain the average value of test points. The computation formula of the real temperature of the terrain ($T_{x,t}$)-based DEM data and the vertical lapse rate is as follows,

$$T_{x,t} = T_{k(x,t)} - 0.01 \times T_t \times H, \quad (12)$$

where H is the altitude and T_t is the vertical decline rate.

3.2.3 Simulating the spatial distribution of solar radiation data

Generally, meteorological stations (even in the mountain area) are located at either the foot or the top of the mountain and have no other features within a certain distance from the shelter. Thus, meteorological data, such as radiation and temperature, are observed in the horizontal plane and as a result, are tremendously affected by the surrounding terrain. Irregular terrain and complex underlying surfaces cause each section of the mountain to accept the solar radiation in tremendously different ways. Thus, solely relying on meteorological observatory data and spatial interpolation methods to describe the precise spatial distribution of total solar radiation in the ARNC with its complex mountainous terrain can generate significant errors. Therefore, by using the DEM as a basis and giving full consideration to the effect of the overlap of different terrains on total solar radiation, the sunshine percentage, the astronomical radiation fit for total solar radiation, and the empirical coefficients, the Angström-Prescott model (APM) is used to calculate total solar radiation of the undulating terrain (see Table 1). In addition, due to the model's relatively low error rates, few input parameters, and ease of obtaining data, it has been the most convenient

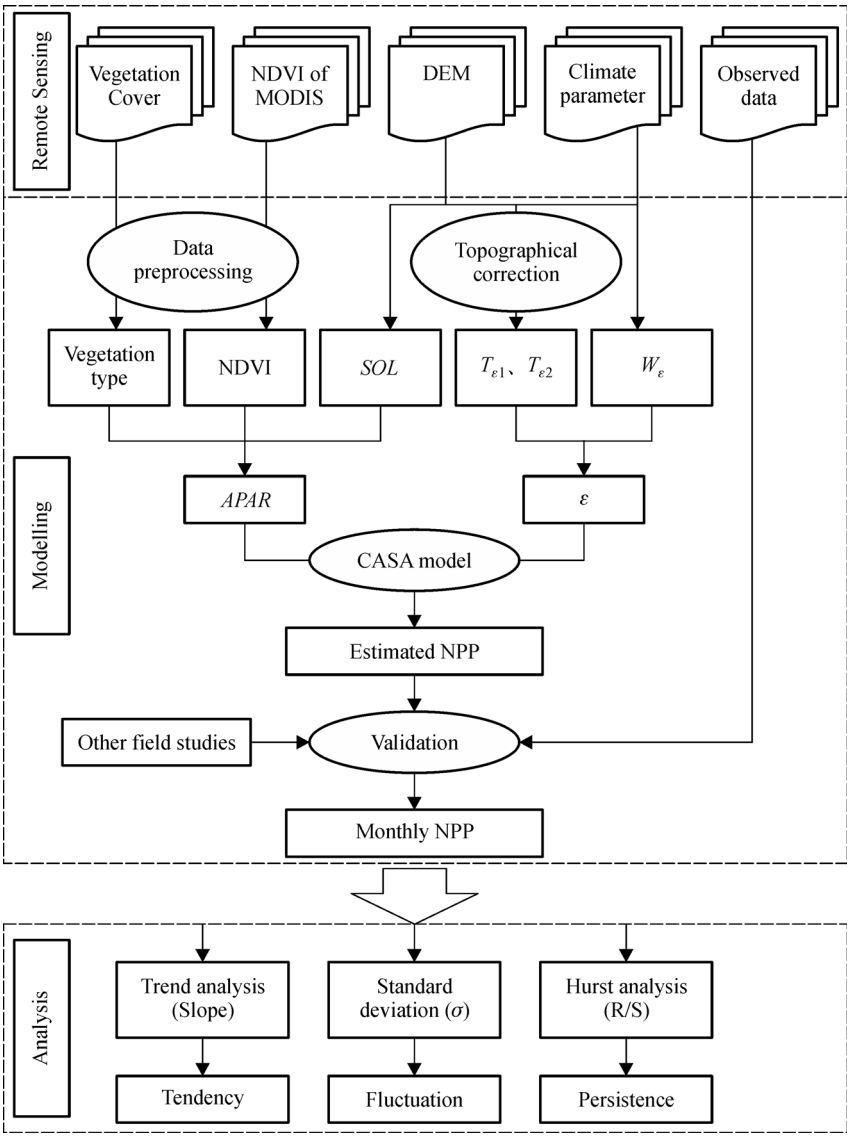

Fig. 2 Flow diagram summarizing the methodology for the Carnegie-Ames-Stanford Approach (CASA) model estimates based on vegetation cover, NDVI , DEM, and Climate parameter. *SOL* = total solar radiation; $T_{\varepsilon 1}$ and $T_{\varepsilon 2}$ = temperature stress coefficients; W_ε = the moisture stress coefficient; *APAR* = photosynthetically active radiation; and ε = light-use efficiency. Trend analysis (slope) can detect and analyze the temporal tendency of each grid in the long time series. Standard deviation (σ) can reflect the fluctuation. The Hurst analysis (R/S) can evaluate the persistence or non-persistence of a time series of the NPP.

Table 1 List of methods used and their functions and references

Name	Functions	Key references
$T_{x,t}$	$T_{x,t}$ interpolates the real temperature of the terrain-based DEM data	Li et al. (2006)
Q_t	Q_t simulates the total monthly solar radiation in the undulating terrain	Angström (1924)
Slope	The slope method detects and analyzes the temporal tendency of each grid	Stow et al. (2007)
σ	σ quantifies the amount of variation or dispersion of a set of data values	Xu (2010)
Hurst index	The Hurst index evaluates the persistence or non-persistence of a time series	Hurst (1951)

and widely used correlation for estimating solar radiation (Angström, 1924; Prescott, 1940; Almorox and Hontoria, 2004; Li et al., 2013a; Liu et al., 2013). The formula is as follows (Liu et al., 2013):

$$Q_t = Q_0(a + b \cdot S), \tag{13}$$

where Q_t is the monthly total solar radiation in the undulating terrain; Q_0 is the monthly astronomical radiation; a and b are the empirical coefficients and were calculated to be 0.22 and 0.773, respectively, in this study; and S is the sunshine percentage.

3.2.4 Trend analysis (slope)

The greenness rate of change (GRC) is defined as the slope of the linear regression line with least squares fit of the inter-annual NDVI values (Stow et al., 2007). The slope of the regression method was applied to detect and analyze the temporal tendency of each grid in the long time series, and some influences on the trend analysis that resulted from abnormal factors were dismissed (see Table 1). Here, we took GRC as an indicator for the trend of NPP images from 2001 to 2012. It was generated with the following formula:

$$\text{Slope} = \frac{n \times \sum_{i=1}^{n} NPP_i - \sum_{i=1}^{n} i \sum_{i=1}^{n} NPP_i}{n \times \sum_{i=1}^{n} i^2 - \left(\sum_{i=1}^{n} i\right)^2}, \quad (14)$$

where i is the ordinal number of the year, from 1 to 12, and n is equal to 12. NPP_i is the mean NPP of year i using the Maximum Value Compositing (MVC) method (Holben, 1986), which can reduce some errors from cloud cover and large solar zenith angles. Positive slopes indicate increasing trends, while negative slopes indicate decreasing trends.

3.2.5 Standard deviation (σ)

The standard deviation (σ) is a measure used to quantify the amount of variation or dispersion of a set of data values (see Table 1). The stability of the NPP from 2001 to 2012 can be evaluated with the standard deviation σ calculated by the following formula:

$$\sigma = \sqrt{\frac{1}{n} \sum_{i=1}^{n} (NPP_i - \overline{NPP})^2}, \quad (15)$$

where $\overline{NPP}$ is the mean of NPP; NPP_i is the NPP in a given year i; and n is the number of data points in the sample. σ values were divided into five levels by using the Natural Fracture method of ARCGIS 10.1: high deviation ($\sigma > 0.026$), relatively high deviation ($0.020 < \sigma \leqslant 0.026$), moderate deviation ($0.015 < \sigma \leqslant 0.020$), relatively low deviation ($0.010 < \sigma \leqslant 0.015$), and low deviation ($0 < \sigma \leqslant 0.010$). The larger the σ values, the greater the change in NPP, and conversely, the lower the σ values, the greater the stability of the NPP.

3.2.6 Hurst method (R/S)

The rescaled-range (R/S) method was introduced by Hurst (1951) as a tool for evaluating the persistence or non-persistence of a time series (see Table 1). R is defined as the difference between the maximum and minimum amounts accumulated for the time series:

$$R(m) = \max_{1 \leqslant m \leqslant n} X(t) - \min_{1 \leqslant m \leqslant n} X(t),$$

$$(m = 1,2,...,n). \quad (16)$$

The range R will typically depend on the time span and normally increases when a larger time span is considered.

The standard deviation is estimated from the time series by:

$$S(m) = \left[\frac{1}{m} \sum_{i=1}^{m} (\Delta NPP_i - \overline{\Delta NPP(m)})^2\right]^{\frac{1}{2}},$$

$$(m = 1,2,...,n), \quad (17)$$

where H is called the Hurst index; its range is 0 to 1. The range $1/2 < H < 1$ indicates that the future trend is the same as the past; in other words, the course has persistence. When H is close to 1, the persistence is strong. When $H = 1/2$, the future is independent of the past and events are random. The range $0 < H < 1/2$ indicates that the future trend is contrary to the past; namely, that this course has anti-persistence. An H value close to 0 indicates that anti-persistence is strong.

4 Results

4.1 Validation of the NPP

To validate the predicted NPP, we first compared the annual mean NPP over the period 2001–2012 from the CASA model and that from observations at 40 sites downloaded from the ORNL DAAC (http://daac.ornl.gov/). The observed annual NPP came from each site's observed average data over 60 years (1946–2006). The results of the estimated NPP and corresponding observed NPP are shown in Fig. 3. Although their time series differ, the CASA model performed fairly well in estimating NPP, showing a high coefficient of determination (R^2) of 0.76. In addition, due to the influence of changing environmental factors such as temperature, precipitation, and human activities, disagreement between estimates and observations was inevitable. In addition, the estimated NPP patterns were mostly located within the range of the observed NPP. The CASA model, therefore, is a good potential tool and can be used for analyzing NPP patterns in the ARNC.

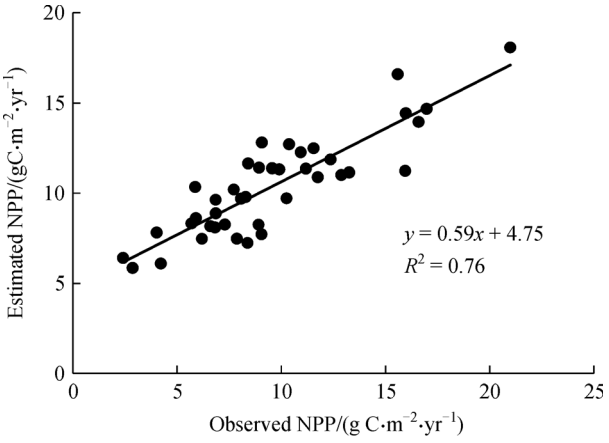

Fig. 3 Comparison of simulated and observed NPP.

The MODIS NPP has been well verified and used to study NPP at regional or global scales in monitoring plant productivity and for estimating biomass and global changes (Silvestri et al., 2002; Running et al., 2004). In China, many researchers have used MODIS NPP data to validate the estimated NPP in the Chinese Loess Plateau (Xie et al., 2014), the Wuling mountainous area (Sun et al., 2015), and the Tibetan Plateau (Mao et al., 2015). Therefore, using the MODIS NPP to validate NPP is a highly reliable method. We compared the estimated NPP with the annual MODIS NPP with a spatial resolution of 1 km×1 km using the BIOME-BGC model and found that they showed similar spatial patterns. The mean annual NPP was higher in the northeast and gradually decreased toward the southwest; however, the values of the MODIS NPP were higher than those of the estimated NPP in 2001, 2003, 2007, and 2010. In other years, the differences between the estimated NPP and the MODIS NPP were very slight, ranging from 3.71 to 24.46 g C·m^{-2}·yr^{-1}. Furthermore, the total annual data of MODIS NPP were similar to the total annual estimated NPP, except in 2001 and 2003. The estimated NPP in 2001 was higher than the MODIS NPP data by 22.47 Mt C ·yr^{-1}. Generally speaking, however, the CASA model could reproduce China's actual NPP reasonably well.

4.2 Spatial and temporal changes in NPP

The spatial patterns of a 12-year mean annual NPP of the ARNC for the period 2001–2012 are illustrated in Fig. 4. The mean annual NPP was observed to be higher in the northeast than in the southwest, with a gradually diminishing trend between the two. The overall mean annual NPP ranged from 2.4 to 1647 g C·m^{-2}, with a 12-year mean value of 803.65 g C·m^{-2}. Partition statistics based on the geographical regions by the physio-geographical regional system were also calculated. Higher NPP values were distributed in the Inner Mongolia temperate steppe region, with an annual average NPP of 953.68 g C·m^{-2}·yr^{-1}; values which were well above the overall annual average NPP value in the region. The Xinjiang Mountain grassland-coniferous forest region also had a higher NPP value, with an annual average of 860.73 g C·m^{-2}·yr^{-1}. The lowest NPP values, however, were in the northwestern warm-temperate desert region, with an annual average of only 703.60 g C·m^{-2}·yr^{-1}. This correlated well with the types and quantity of vegetation (Fig. 5). Primary vegetation types were needle-leaf forest, broadleaf forest, and grassland in the eastern ARNC as well as the Tianshan and Altay mountains (areas of high vegetation cover), while the central and western regions were typified as mostly barren and sparsely vegetated.

The NPP in the ARNC shows an obvious regularity with the seasons. From March to September, the NPP values were higher than those in the other months. The average

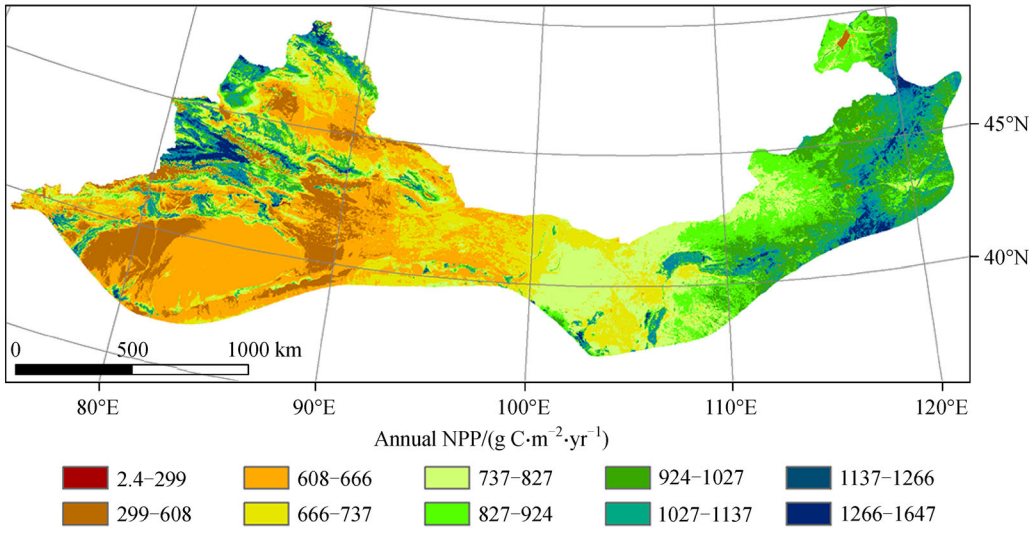

Fig. 4 Spatial distribution of mean annual NPP of the ARNC from 2001 to 2012.

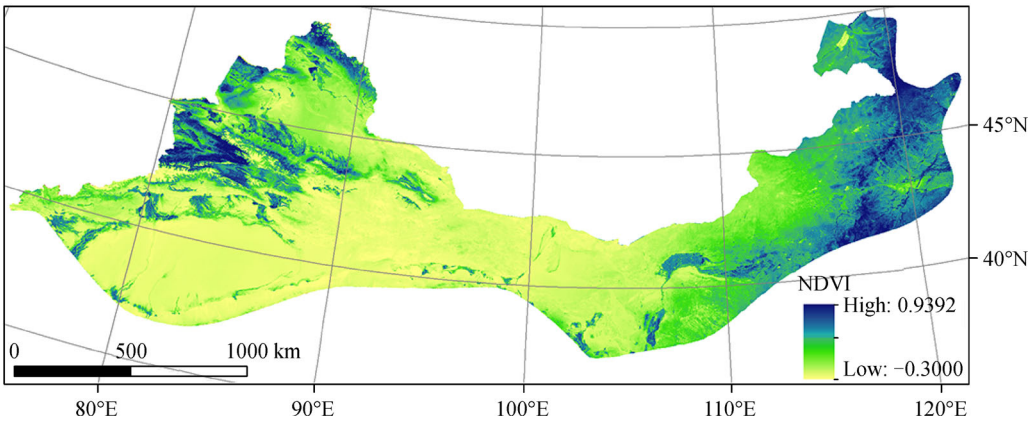

Fig. 5 Spatial distribution of mean annual NDVI of the ARNC from 2001 to 2012.

NPP in January was only 27.81 g C·m^{-2}, while it was highest during the growing season in July at 120.11 g C·m^{-2}. The annual NPP value was the lowest in December at 22.85 g C·m^{-2}, and the lowest monthly average NPP value was 20.12 g C·m^{-2} in December 2012.

The overall mean annual NPP ranged from 789.14 to 829.15, while the mean annual NPP fluctuated at an increasing rate of 2.327 g C·m^{-2}·yr^{-1} from 2001 to 2012 (Fig. 6). After 2010, this increasing trend markedly accelerated, with an annual increase of 21.19 g C·m^{-2}·yr^{-1}. Compared with the mean annual NPP in 2001, the value in 2012 grew 37.86 g C·m^{-2}. Over the entire 12-year period, the lowest mean annual NPP was 789.14 g C·m^{-2}·yr^{-1} in 2006, while the highest was 829.15 g C·m^{-2}·yr^{-1} in 2012.

4.2.1 Change trends in NPP

The slope reflects the spatial change trend of NPP, which is defined as the linear regression line. The overall NPP of the ARNC showed a higher tendency towards (Fig. 7) improvement than degradation over the 12 year period. From 2001 to 2012, the area of NPP degradation covered 49.77×10^4 km^2, accounting for 18.58% of the total area, while the area of improvement was 137.86×10^4 km^2, comprising almost half of the ARNC.

The regions of NPP degradation were mainly located in the Xilingol Grassland Nature Reserve, the Inland River Basins in the Hexi Corridor, and similar areas — those seriously affected by human activities such as deforestation and overgrazing. The partial NPP pixels exerted an increasing trend in the northeast of Inner Mongolia and the three basins in Xinjiang. Land-use and land-cover changes were the major causes. For instance, some grassland was transformed into farmland. When the negative consequences of grassland desertification became clear, a series of protection measures were established to provide favorable conditions for grassland restoration, such as grassland preservation, reasonable grazing, and other measures. The NPP in the Tianshan, Altay, and Great Khingan mountain ranges also showed increases after these measures were implemented. In addition, the vegetation in these areas was only slightly affected by human activity yet growth was promoted by precipitation, snow melt, and glacier.

The NPP in the Inner Mongolia temperate steppe region

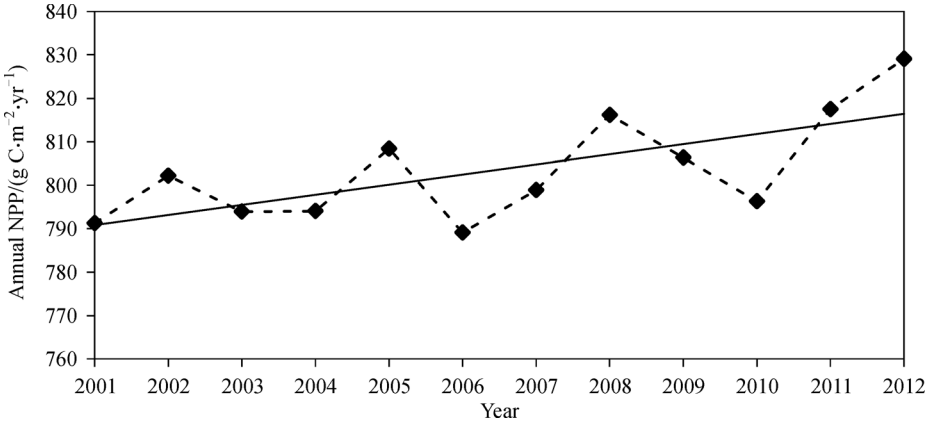

Fig. 6 Interannual variations in total NPP over the ARNC from 2001 to 2012.

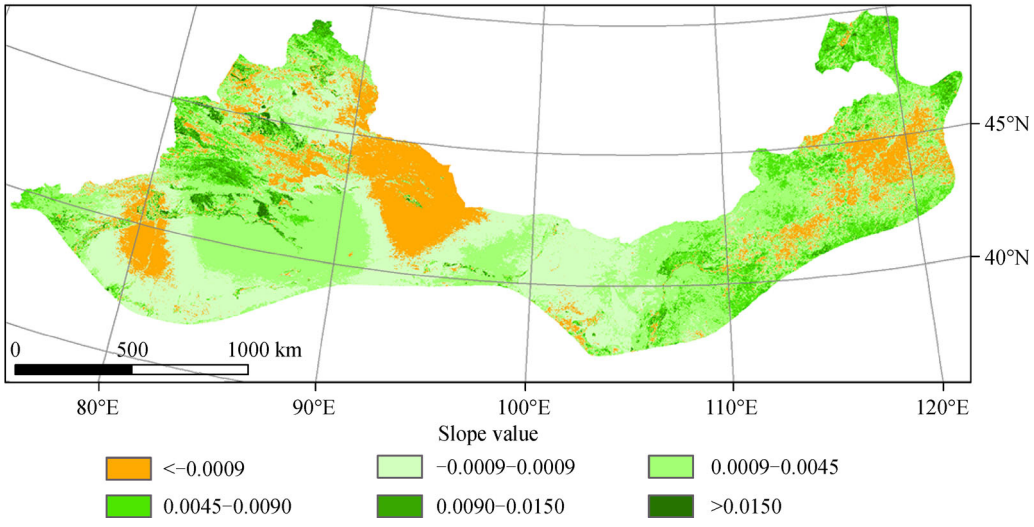

Fig. 7 Distribution of the linear trend of annual NPP changes in the ARNC from 2001 to 2012.

showed the largest area of increase. The improved area was 137.84×10^4 km^2, accounting for 71.41% of the total area of Inner Mongolia, while the area of NPP degradation was 10.54×10^4 km^2, accounting for only 16.12%. In the northwestern warm-temperate desert region, almost half (42.81) of this area's NPP was unchanged yet the area of degradation was 28.01×10^4 km^2, accounting for 19.01% of the region. The area where NPP changed dramatically was in the Xinjiang Mountain grassland-coniferous forest region. The area of degradation was 8.11×10^4 km^2, accounting for 22.58%, the area of improvement was 21.15×10^4 km^2, accounting for 58.83%, and the area of unchanged NPP was only 18.59% of the total area.

4.2.2 Changes in the stability of NPP

The NPP data obtained using the MVC method were used to analyze the fluctuant characteristics of NPP from 2001 to 2012 in the ARNC (Fig. 8). The standard deviation (σ) varied from 0.001 to 0.235, and overall its characteristics were "more high deviation and less low deviation," although the stability of the NPP showed significant regional differences. The regions of high deviation occurred around 105°E and 42°N in the northern area, occupied 56% of the total area, and anastomosed with the improved area. The proportions of high and medium deviation were relatively small — only 14.10% of the research area — and randomly distributed in the ARNC. The area of low deviation was 72.08×10^4 km^2, mainly concentrated in the Tarim, Junggar, and Qaidam basins, and in Alashan where the major vegetation types were desert plants showing a patchy distribution pattern. Here, the change in NPP was relatively stable.

Divisional statistics showed that the changing trend of NPP in the three subareas of the ARNC were in keeping with the overall trend of the ARNC and were mostly consistent with the improved regions of the overall NPP. The highest proportion of high-deviation NPP was located in the Inner Mongolia temperate steppe region — up to 79.34% of its own total area. The second-largest area of high NPP deviation, namely the Xinjiang Mountain grassland-coniferous forest region, was relatively large, reaching 22.48×10^4 km^2 or 62.55% of its own total area. By contrast, the area of high NPP deviation in the northwestern warm-temperate desert region was the smallest, accounting for only 22.44% of its own total area. However, this region's low deviation area was as high as 20.20%, far higher than either the Xinjiang Mountain grassland-coniferous forest region (3.02%) or the Inner Mongolia temperate steppe region (0.12%), due to the sparse vegetation of the northwestern warm-temperate desert region, the influence of human activity, and the inconspicuous meteorological factors in this area. The vegetation cover in the two remaining subareas, however, was mostly forest, farmland, and other green landscape types — vegetation that is very sensitive to the changing climate and anthropogenic activities and prone to volatility.

4.2.3 Change persistence in NPP

Annual NPP data obtained monthly from 2001–2012, using the MVC method, were computed using the Hurst index of NPP with MATLAB and ARCGIS software (Fig. 9). The Hurst index values were in the range of 0.11–1.00; the average value was 0.55. The area where the Hurst index value was less than 0.25 comprised only 0.20% of the total research area, showing that the anti-persistence of NPP was very weak and could be ignored. For the remainder, the Hurst index values were divided into weak, medium, and strong persistence, according to the thresholds < 0.5, 0.5–0.65, and > 0.65, respectively. As a whole, the area of strong persistence comprised 25.88×10^4 km^2,

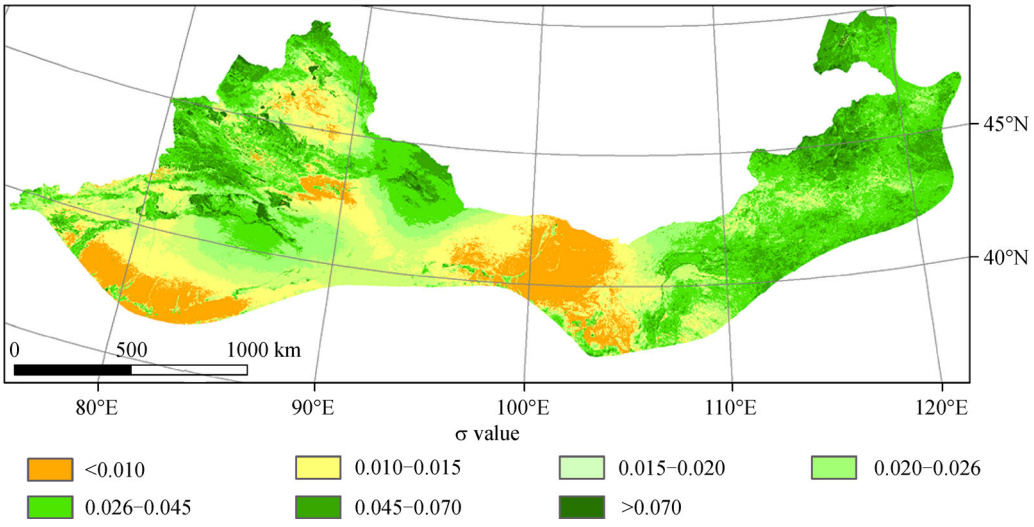

Fig. 8 Standard deviation of NPP changes in the Northwest arid region from 2001 to 2012.

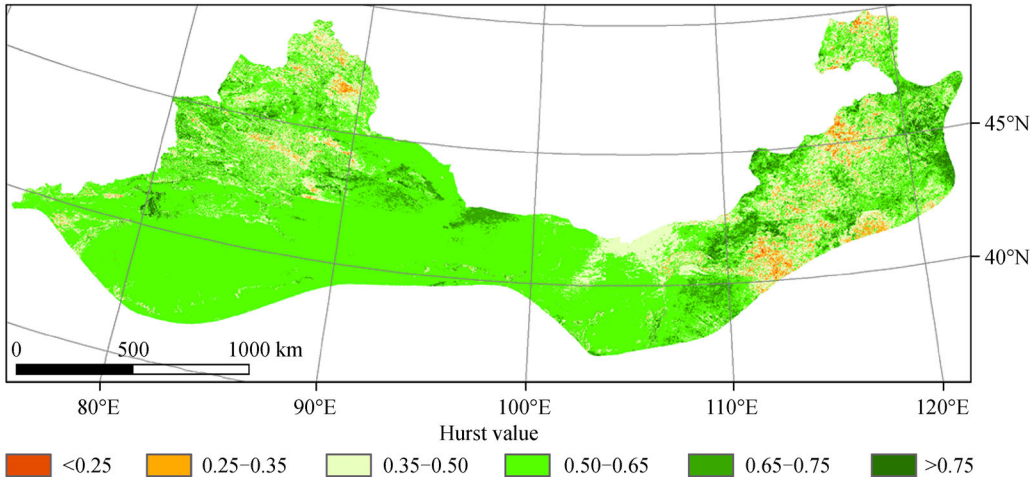

Fig. 9 Hurst index of NPP changes in the northwest arid region from 2001 to 2012.

accounting for 9.66% of the total study area, and was mainly distributed in the Root Flag, the Laura Left Flag, the Siziwang Banner, and a few smaller areas. The area of medium persistence accounted for 67.85% of the ARNC and was found in the Mesozoic-Cenozoic, La Shan Left Flag, and a few other areas. The area of weak persistence comprised 60.28×10^4 km^2 and primarily occupied West Ujimqin, Laura Right Flag, and Low-Amphibolite. Overall, the wide range of medium and strong persistence indicates that although the vegetational developmental trend can be expected to continue to improve, it still faces risks and uncertainties.

At the regional scale, the Hurst index showed a similar trend in the three subareas, namely, that the medium persistence area was the most widespread, the weak persistence area was intermediate, and the strong persistence area was the least. Most areas of the northwestern warm-temperate desert region showed characteristics of medium and weak persistence; up to 95.25% of the region fell within this category. The lowest proportion of medium and weak persistence area was in the Xinjiang Mountain grassland-coniferous forest region. This type comprised 88.73% of this region. More persistence was found, however, in the Inner Mongolia temperate steppe region. Compared with the other regions, the Inner Mongolia temperate steppe is a major agricultural and pastureland interlaced region, and its ecological system is more stable, its vegetation recovery ability strong, and its sustainability significantly higher than that of the other two subareas. By contrast, the northwestern warm-temperate desert region has experienced serious desertification, and its environment is very fragile, so that its overall persistence has been poor. Future regional restoration efforts should be focused on strengthening the stability of this ecosystem.

To further explore the change trends and persistence of NPP in the ARNC, we carried out a spatial overlay analysis of the slope value of the linear regression line and Hurst index using the geographical information system software Arc/Info, and we mapped persistence change trends by combining these data using ARCGIS software. There were nine distribution types: improvement and strong persistence, improvement and medium persistence, improvement and weak persistence, stability and strong persistence, stability and medium persistence, stability and weak persistence, degradation and strong persistence, degradation and medium persistence, and degradation and weak persistence (Fig. 10). The proportions of area showing improvement and strong persistence, improvement and medium persistence, and degradation and weak persistence were 5.59%, 32.26%, and 4.20%, respectively, together accounting for 42.05% of the total study area. From these percentages, it can be seen that change trends for NPP are not optimistic and leave much room for improvement. The area of stability was 80.34×10^4 km^2: 29.97% of the region. The proportion of the areas of improvement and weak persistence and of degradation and strong persistence was 15.91%, mainly distributed in Barr Tiger Flag, Right Flag, Chen low-amphibolite, Altay City, the northern part of Hami City, and Mazong Mountain in Subei County.

The development trend of NPP was mainly benign. The proportions of areas showing improvement and strong persistence, improvement and medium persistence, and improvement and weak persistence were 13.59%, 32.56%, and 5.59%, respectively, occupying 51.44% of the ARNC area and mainly distributed in the center of Xinjiang, the middle of the Hexi corridor in Gansu province, and major regions of Inner Mongolia, such as Laura Left Flag, Laura Right Flag, and the eastern part of Erdos City. The area of stability was the largest, with a ratio of approximately 30%, and the trend of persistence was normal. These regions of degradation and strong persistence and of degradation and medium persistence were distributed in the boundaries along Gansu Province, Xinjiang Autonomous Region, and Inner Mongolia Autonomous Region, and were scattered near the center of the Tianshan Mountains, the eastern part of Xilingol League, the grasslands along the Xi Liao River, and in the Altai Mountains. These areas should be a priority for ecological protection regulations.

In the Inner Mongolia temperate steppe region, the proportion of improved regions — including strong, medium and weak persistence — was 71.41%, obviously showing that the development trend of NPP was favorable and positive in this region. Following this was the Xinjiang Mountain grassland-coniferous forest region, with an approximate proportion of 58.82%. Its NPP value also shows positive development. In contrast, the ratio of the Inner Mongolia temperate steppe region was only 38.18%, due to weak vegetation restoration ability that can be ascribed to the changing climate as well as natural factors. However, it is important to note that although the development trend of NPP was good overall, areas of degradation and strong persistence and of improvement and weak persistence totaled 25.52×10^4 km^2, comprising 30.19% of the Inner Mongolia temperate steppe region. This region, therefore, needs more attention, with restrictions that could promote vegetation restoration and other ecological protections.

5 Discussion

A precise evaluation of NPP at the regional or global scale is always difficult. In this study, we first compared the annual mean NPP with NPP data from the 40 downloaded

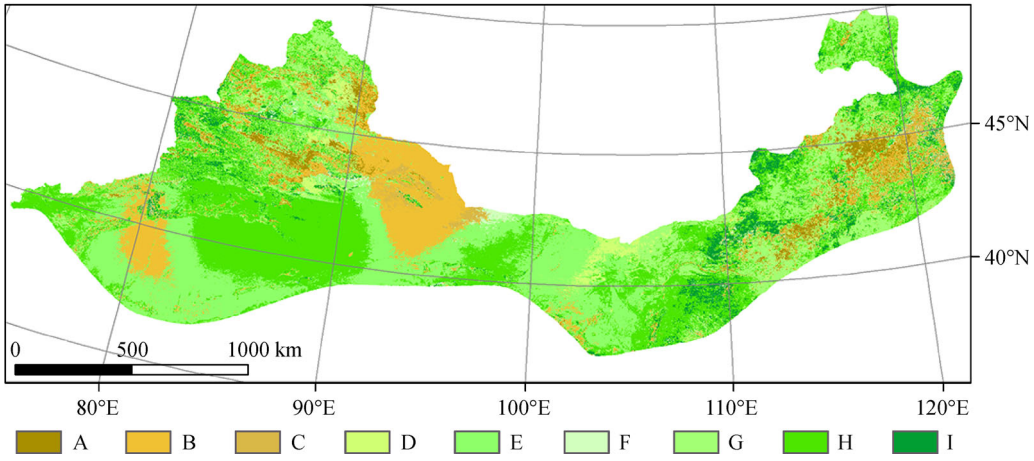

Fig. 10 Spatial change characteristics of NPP based on the trends and the Hurst index. Note: nine distribution types are present. A: improvement and strong persistence; B: improvement and medium persistence; C: improvement and weak persistence; D: stability and strong persistence; E: stability and medium persistence; F: stability and weak persistence; G: degradation and strong persistence; H: degradation and medium persistence; I: degradation and weak persistence.

sites. In general, the CASA model performed fairly well in estimating NPP, showing a coefficient of determination (R^2) of 0.76. These data, it should be noted, did not consider the error resulting from temperature, precipitation, or human activities. Even though the acquisition of observed NPP is difficult, the resulting data from the sites is difficult to extrapolate to regional and global scales. Furthermore, different time periods were used for the estimated vs. the observed data; the period of the estimated NPP was 2001 to 2012, while the observed was 1946 to 2006. We also do not know if the observed NPP data are representational. If not, the differences may be greater and it would be impossible or impractical to determine their correlations. Moreover, validation was only performed at the annual scale, not at seasonal or regional scales. This presents a limitation, and thus multiscale observed data should be obtained for a more precise validation. Human activities should be separated from the environment before performing the NPP validation, a step which unfortunately was not taken, creating a major disadvantage. In fact, actual NPP values may still not be accurately estimated under the existing conditions for this technique. Even so, it is possible to compare the mean NPP values for large samples and to study the spatiotemporal dynamics of regional NPP with some precision (Matsushita and Tamura, 2002).

The estimated NPP can also be compared with the MODIS NPP (i.e., MOD17A3). MODIS NPP is one of the MODIS global ecological parameters available from the University of Montana Numerical Terradynamic Simulation Group (NTSG), and has been widely recognized and applied at the global scale. Previous studies have shown that MOD17A3 can also be applied with some accuracy in China. Guo et al. (2008) compared 128 measured forest data points with the average MOD17A3 NPP from 2000 to 2006 and found that although the measured data points were slightly higher than those from the MOD17A3 NPP, there was a close correlation between them. Zhao et al. (2011) used the GLOPEM-CEVSA model to simulate NPP in northeast China from 2000 to 2008, which, when compared with MOD17A3, found that $R^2 = 0.525$, $P < 0.001$. In addition, many researchers, such as He et al. (2006), Guo et al. (2008), Li et al. (2013a), and Wang et al. (2013), used MODIS NPP data in the South-North Water Diversion Project, northeast China, Henan Province, Jiangsu Province, and other regions to analyze the temporal-spatial distribution characteristics of the vegetation NPP. It is reasonable, therefore, for this study to compare the estimated NPP with the MODIS NPP to explain the respective trend analysis of the reliability of the data source. Our results show similar spatial patterns; namely, that the mean annual NPP in the northeast was higher than that in the southwest. The differences between the estimated NPP and the MODIS NPP were very small, within the range of 3.71 to 24.46 g $C \cdot m^{-2} \cdot yr^{-1}$. This evidence further illustrates that the CASA model presents a highly reliable method of calculating NPP.

Although our validation results at 40 sites showed an overall good performance of the CASA model for estimating NPP in the ARNC, there were some unavoidable uncertainties. For example, different models required different input parameters and theoretical models were somewhat compromised. Researchers have developed numerous models and methods for estimating NPP, with both advantages and disadvantages; yet to date, no single universal model has been found for estimating NPP. Although we were able to improve the CASA to some extent by using some static parameters either obtained or calculated in small experimental regions, and were able to monitor data from a few experimental stations in the model, errors inevitably resulted when data were applied to large-scale regions. In addition, the observed data were difficult to obtain and validate, and the estimated data introduced some uncertainties. For example, the measured NPP obtained from the global NPP database was based on a different time period than that for the estimated NPP. Even though we used the average annual data, temporal differences led to deviations in estimating biomass. The measured NPP came from monitored values from the needle-leaf forests, temperate forests, and grasslands of northern China, while the corresponding measured data came from the ubiquitous sparse vegetation types the arid areas were lacking. The low spatial resolution of MODIS NPP may have generated a large number of mixed pixels that affected the precision and made NC verification difficult. Thus, in the future, more time and money should be invested to improve and enhance the precision of NPP validation and to reduce the uncertainties as much as possible.

One minor problem with the model may be that the leaf area index (LAI) and photosynthetic active radiation (FPAR) showed a saturation problem in some areas. However, because this study focused on the change in vegetation net primary productivity throughout the year, the FPAR and LAI saturation phenomenon are understandable (Jiang et al., 2011). This study modeled NPP values from different vegetation types in comparison with the research of Zhu et al. (2005) and Ren and Liu (2013) (comparison data are shown in Table 2). The results show similar overall NPP trends. The NPP values for needle-leaf forest and broadleaf forest were lower than the estimated values from Zhu et al. (2005), while our brush, grassland, and farmland NPP values were higher. Relatively speaking, the estimated NPP of brush and grassland were lower than those from Ren and Liu (2013), while the NPP values of the remaining vegetation types were higher. This phenomenon can be explained as follows. 1) Each study covered a different research region- Zhu et al. (2005) covered the Inner Mongolia region of China, Ren and Liu (2013) covered Northwest China and our research took place in the ARNC. 2) Each study covered a different time period- Zhu et al. (2005) covered 2002, Ren and Liu (2013) covered 2000, 2003, 2006 and 2009, and our study

covered the period of 2001 to 2012. 3) The input parameters were different. 4) The meteorological stations from which our data were obtained were small and poorly distributed throughout the study area. Although interpolation methods for gathering meteorological data have improved over the last decade, further development is needed to enhance the precision and effectiveness of the model. Finally, some of the differences in the results could have been caused by human interference. As observed in the various research areas, the distribution pattern of the NPP remained consistent in the ARNC. Wang et al. (2014) estimated the NPP of Gansu Province, Northwest China in 2003. They observed greater NPP values centralized in the high altitude areas covered with growing forest and grassland, whereas lower NPP was distributed across the Hexi Corridor and Northern Mountains characterized by sparse vegetation. Meanwhile, the evident seasonal trend of NPP was higher in summer than in winter. These research results are highly consistent with our study. Li et al. (2013b) studied the NPP characteristics and changes in the Inner Mongolia Autonomous Region from 2003 to 2008. They found that the NPP decreased from northeast to southwest and that the period from May to September accounted for 84.2% of the annual NPP. Our research shows that the NPP values from March to September were higher than those in other months. The distribution trend of the NPP is also in line with the research of Li et al. (2013b). Furthermore, the spatial distribution of NPP in the Xinjiang Autonomous Region of the ARNC was clearly heterogeneous. High values were distributed in the Altai Mountains and Tianshan Mountains with abundant water resources and meadows, including alpine and subalpine meadows. These results are in accord with the outcomes reported by Zhou et al. (2014). Although the distribution pattern of NPP is consistent with others' achievements, many differences can be found when delving deeper. The estimation of NPP entails vast and abundant uncertainties, requiring greater effort crucial for reliable model development.

In summary, differences in the use of remote sensing data, vegetation classification data, model and research dimensions, as well as the possibility of system error, could cause differences in the NPP values calculated by the different studies. Clearly, some improvements in the study methods are needed for more consistent results. Further study is needed on the physiological mechanisms used for calculating NPP which is influenced by both environmental and botanical factors. A deeper understanding of these factors is crucial to bring the NPP estimation model more in line with these physical realities.The remote sensing software will also need to be updated to reflect our increased knowledge of these environmental and biological mechanisms. Despite the drawbacks of the current models, the MODIS NPP from this study and the results of other researchers demonstrate an overall good performance for the CASA model in estimating NPP in the ARNC.

Therefore, the estimated NPP derived from the CASA model results were analyzed regarding spatial, monthly, and inter-annual variations. From a spatial distribution perspective, the gradient distribution of NPP in the ARNC is distinct, while the NPP in the northeast regions was generally higher than that in the southwest region due to the spatial variability in precipitation and temperature. Analyses of annual NPP variability showed an obvious increasing trend over time. Notable monthly variations in the NPP were observed and were primarily accumulated between May and August. This is likely due to the abundant solar radiation and favorable hydrothermal conditions with the concentrated herbaceous plant growth during this period. Plant growth is slow from March to April and from September to October when temperatures are low. Plant growth grinds to a halt from November through the following February. As a result, the NPP is very low during this period of decreased vegetation. This phenomenon indicates that a suitable combination of water (precipitation) and thermal regimes is a principal driver for dynamic change in NPP.

Increased studies on the effectiveness of government policies and programs that monitor the impact of human activities on NPP are of significant importance. For example, the NPP values of the Ejin Banner were significantly improved, due to the government's decision in 2000 to transfer water downstream, which in turn led to an increase in water levels and in vegetation. Mu et al. (2013b) reported that the NPP has significantly increased in the Mu Us Sandy Land, the Ala Shan Desert, and the Otindag Sandland under a series of positive measures taken by the government. The regions of the Wulate Midum Banner, Holingol Banner, Sizhiwangqi Banner, and Ejin Horo Banner launched a pilot project for soil and water conservation and ecosystem restoration. As a result, cropland was returned to grassland or woodland, which prohibited grazing, encouraged pen raising, and a forest shelter belt was constructed to control soil erosion and grassland degradation from 2001 to 2002. The environment and the NPP of these regions have immensely improved. Due to the rapid growth of the pastoral population and the high-speed development of our social economy over the past 30 years, the pressure on the grassland has significantly increased, as has the severity of overgrazing, contributing to the degradation of grassland. Significant grassland degradation will bring about a decline in primary productivity. The light, moderate, severe or extreme degradation of grassland is expected to see primary productivity fall by 20%–30%, 35%–60%, 60.85%, or 85%, respectively (Zheng et al., 2005). The NPP in the Tianshan Mountains, the eastern part of Xilingol League, the grasslands of the Xi Liao River valley, and the Altai Mountains has significantly and persistently decreased, perhaps due to grassland degradation. In spite of the drastic measures taken in the Xilingol League (e.g., grazing in spring, enclosed grazing, and

blocking of rotational grazing), which have shown some success, the region still faces grassland degradation, land desertification, and numerous other environmental issues. As a result, the NPP of the region continues to decline. Hence, the improvement of governmental measures and policies in the ARNC is critical to protect the environment and improve the primary productivity.

The method of standard deviation (σ) describes the variability of NPP for an image pixel in many years. Many researchers have used this method to uncover the NPP variability range in response to human activities. Reeves et al. (2014) modeled the standard deviation of the mean slope of the linear regression of the NPP trend to 2100 for three emission scenarios. Ren and Liu (2013) calculated the inter-annual standard deviation of the vegetation NPP value in Northwest China. They concluded that the Xinjiang had a low standard deviation and that the fluctuation was insignificant and not obvious. This desert area is characterized with sparse vegetation, and affects from human activities are minimal. The North Shaanxi Loess Plateau had large fluctuations due to the destruction of the ecological environment influenced by human activities. These conclusions are in line with ours. In this paper, high-deviation NPP was located in the Inner Mongolia temperate steppe region, and the vegetation and climate conditions were superior and favorable. Thus, these regions were suitable for human life. The deviation of the NPP was immense in the Inner Mongolia temperate steppe region. In contrast, the area of high NPP deviation in the northwestern warm-temperate desert region was the smallest, accounting for only 22.44% of its own total area. The land cover areas were small, primarily within the Gobi desert, and unsuitable for human habitation. As a result, the affect from human activities was again minimal, with the variability of NPP related to anthropogenic activities. In this paper, we discuss the effects of climatic variables and human activities on NPP, which poses both limitations and drawbacks. Because the influencing factors are multifarious and complicated, both natural factors (e.g., radiation, evaporation, and carbon dioxide concentration) and anthropogenic factors (e.g., grazing and enclosure) must be fully taken into account to clarify the effects of climate change and anthropogenic activities on the NPP in the future. Thus, this will be the focus of my ongoing research.

One result from this study is clear: the regions distributed along the boundaries of Gansu Province, Xinjiang Autonomous Region, and Inner Mongolia Autonomous Region, and those scattered in the center of the Tianshan Mountains, the eastern part of Xilingol League, the grasslands of the Xi Liao River valley, and the Altai Mountains need the attention of ecological protection agencies due to their characterization of 'degradation and strong persistence' and 'degradation and medium persistence.' The results of this study show that detailed analyses of NPP data have derived valuable information about the ARNC and can provide significant information based on the vegetation growth in the area. These analyses could also provide some suggestions to extend to other arid environments, where both similarities and differences in vegetation productivity have been identified.

6 Conclusions

In this study, the CASA model, in combination with long-term MODIS NDVI series and concurrent meteorological data, was used for NPP modeling in the ARNC for the period 2001–2012. The NPP results were analyzed with regard to spatial and temporal variations at both pixel and regional scales. The derived datasets provided information about the spatial distribution and temporal variation of NPP for the arid environment in the ARNC. The main conclusions can be summarized as follows:

1) The CASA model performed well in the ARNC. The validation results showed that the coefficient of determination (R^2) was 0.76 between the estimated and the observed NPP, and the typical vegetation NPP was similar over trends compared with other field studies.

2) The annual NPP in the ARNC showed evident spatial gradients, with the NPP in the eastern regions generally higher than that in the western areas; a result that can be explained mainly by spatial variability in precipitation.

3) Over the entire study period, the annual NPP showed a significant increasing trend, with an annual average increase of 2.327 g C. However, the increasing trends in

Table 2 Typical vegetation NPP average contrasts (g $C \cdot m^{-2} \cdot yr^{-1}$)

Vegetation type	Present study	Zhu et al. (2005)	Ren and Liu (2013)
Needle-leaf forest	1075.18	900.8−1435.9	735.41−881.99
Broadleaf forest	883.59	1085.6	735.41−881.99
Bush	879.36	235.6	312.13−1242.93
Barren	270.02	19.4	59.78
Grassland	631.56	259.9	700.42−846.86
Farmland	892.19	376.8	414.73
Water	358.67	369	61.98−291.67

NPP were not continuous throughout the 12-year period. Annual NPP showed two trends: a decreasing trend from 2001 to 2005 and an increasing trend from 2006 to 2012. In 2006, the annual NPP reached its minimum value of 789.14 g $C \cdot MJ^{-1}$. This turning point in the trend was associated with a shift in climatic conditions as well as extensive drought events in the region.

4) The standard deviation (σ) varied from 0.001 to 0.235, yet overall, its characteristic was "more high deviation and less low deviation," even though the NPP trend showed significant regional differences. The rate and amplitude of change varied over three subareas, but overall, the trends were consistent with that of the region as a whole.

5) An analysis of the Hurst index showed that the NPP development trend was of medium and strong persistence, and its share of area reached 77.50%. In addition, the development trend of NPP was favorable and positive in the Inner Mongolia temperate steppe region and the Xinjiang mountain grassland-coniferous forest region. However, because of changes in climate and other natural factors, the development trend for the northwestern warm-temperate desert region was not optimistic.

6) The proportion of the areas of either weak improvement and persistence, or of strong degradation and persistence, was 15.91%, mainly distributed in Barr Tiger Flag, Right Flag, Chen low-amphibolite, Altay City, the northern part of Hami City, and Mazong Mountain in Subei County. Thus, they urgently need the direct attention of the government. Alternatively, stronger measures of protection are needed in the regions located in the center of Xinjiang, the middle of the Hexi corridor in Gansu province, and Inner Mongolia (i.e., Laura Left Flag, Laura Right Flag, and the eastern section of Erdos City) to maintain the strong and persistent improvement observed in these areas.

References

Almorox J, Hontoria C (2004). Global solar estimation using sunshine duration in Spain. Energy Convers Manage, 45(9–10): 1529–1535

Angström A (1924). Solar and terrestrial radiation. Report to the international commission for solar research on actinometric investigations of solar and atmospheric radiation. Quart J Roy Met Soc, 50 (210): 121–126

Calvão T, Palmeirim J M (2004). Mapping mediterranean scrub with satellite imagery: biomass estimation and spectral behaviour. Int J Remote Sens, 25(16): 3113–3126

Cao M, Prince S D, Small J, Goetz S J (2004). Remotely sensed interannual variations and trends in terrestrial net primary productivity 1981–2000. Ecosyst, 7(3): 233–242

Chen F J, Shen Y J, Li Q, Guo Y, Xu L M (2011). Spatio-temporal variation analysis of ecological systems NPP in China in past 30 years. Sci Geogr Sin, 31(11): 1409–1414 (in Chinese)

Esser R, Fineschi S, Dobrzycka D, Habbal S R, Edgar R J, Raymond J C, Kohl J L, Guhathakurta M (1999). Plasma properties in coronal holes derived from measurements of minor ion spectral lines and polarized white light intensity. Astrophys J, 510(1): 63–67

Eswaran H, Lal R, Reich P F (2001). Land degradation: an overview. In: Bridges E M, Hannam I D, Oldeman L R, Pening de Vries F W T, Scherr S J , Sompatpanit S, eds. Responses to Land Degradation. Proceedings of the 2nd International Conference on Land Degradation and Desertification, Khon Kaen, Thailand. New Delhi: Oxford Press, 20–35

Fang J Y, Piao S L, Field C B, Pan Y D, Guo Q H, Zhou L M, Peng C H, Tao S (2003). Increasing net primary production in China from 1982 to 1999. Front Ecol Environ, 1(6): 293–297

Field C B, Randerson J T, Malmström C M (1995). Global net primary production: combining ecology and remote sensing. Remote Sens Environ, 51(1): 74–88

Guo Z X, Wang Z M, Zhang B, Liu D W, Yang G, Song K S, Li F (2008). Analysis of temporal-spatial characteristics and factors influencing vegetation NPP in northeast China from 2000 to 2006. Resources Science, 30(8): 1226–1235 (in Chinese)

Haxeltine A, Prentice I C (1996). BIOME3: an equilibrium terrestrial biosphere model based on ecophysiological constraints, resource availability and competition among plant functional types. Global Biogeochem Cycles, 10(4): 693–709

He Y, Dong W J, Guo X Y, Cao L J, Feng D (2006). Terrestrial NPP variation in the region of the South-North Water Diversion Project (East Route). Adv Clim Change Res, 2(5): 246–249 (in Chinese)

Hicke J A, Asner G P, Randerson J T, Tucker C, Los S, Birdsey R, Jenkins J C, Field C, Holland E (2002b). Setellite-derived increases in net primary productivity across North America, 1982–1998. Geophys Res Lett, 29(10): 69-1–69-4

Hicke J A, Asner G P, Randerson J T, Tuker C, Los S, Birdsey R, Jenkins J C, Field C (2002a). Trends in North American net primary productivity derived from satellite observations, 1982–1998. Glob Biogeochem Cy, 16(2): 2-1–2-14

Holben B N (1986). Characteristics of maximum-value composite images from temporal AVHRR data. Int J Remote Sens, 7(11): 1417–1434

Hurst H E (1951). Long term storage capacity of reservoirs. Trans Am Soc Civ Eng, 116(12): 776–808

Jiang R Z, Li X Q, Zhu Y G, Zhang G Z (2011). Spatial-temporal variation of NPP and NDVI correlation in wetland of Yellow River Delta based on MODIS data. Acta Ecol Sin, 31(22): 6708–6716 (in Chinese)

Knorr W, Heimann M (1995). Impact of drought stress and other factors on seasonal land biosphere CO_2 exchange studied through an atmospheric tracer transport model. Tellus B Chem Phys Meterol, 47 (4): 471–489

Li E Z, Tan K, Du P J, Jiang D E (2013a). Net primary productivity of vegetation estimation and correlation analysis based on multi-temporal remote sensing data in Xuzhou. Remote Sensing Technology and Application, 28(4): 689–696 (in Chinese)

Li J, Cui Y P, Liu J Y, Shi W J, Qin Y C (2013b). Estimation and analysis of net primary productivity by integrating MODIS remote sensing data with a light use efficiency model. Ecol Modell, 252(1): 3–10

Li J, You S C, Huang J F (2006). Spatial interpolation method and spatial

distribution characteristics of monthly mean temperature in China during 1961–2000. Ecol Environ, 15(1): 109–114 (in Chinese)

Lin H L (2009). A new model of grassland net primary productivity (NPP) based on the integrated orderly classification system of grassland. The sixth international conference on fuzzy systems and knowledge discovery. Tianjin, China, 52–56

Liu C M, Chen Y N, Xu Z X (2010). Eco-hydrology and sustainable development in the arid regions of China. Hydrol Processes, 24(2): 127–128

Liu C Y, Dong X F, Liu Y Y (2015). Changes of NPP and their relationship to climate factors based on the transformation of different scales in Gansu, China. Catena, 125: 190–199

Liu J Y, Liu M L, Zhuang D F, Zhang Z X, Deng X Z (2003). Study on spatial pattern of land-use change in China during 1995–2000. Sci China Ser D, 46(4): 373–384

Liu Y A, Huang B, Yi C G, Cheng T, Yu J, Qu L A (2013). Simulation by remote sensing and analysis of net primary productivity of vegetation based on topographical correction. Trans Chin Soc of Agric Eng, 29: 130–141 (in Chinese)

Malmström C M, Thompson M V, Juday G P, Los S O, Randerson J T, Field C B (1997). Interannual variation in global-scale net primary production: testing model estimates. Global Biogeochem Cycles, 11 (3): 367–392

Mao D H, Luo L, Wang Z M, Zhang C H, Ren C Y (2015). Variations in net primary productivity and its relationships with warming climate in the permafrost zone of the Tibetan Plateau. J Geogr Sci, 25(8): 967–977

Matsushita B, Tamura M (2002). Integrating remotely sensed data with an ecosystem model to estimate net primary productivity in East Asia. Remote Sens Environ, 81(1): 58–66

Moleele N, Ringrose S, Arnberg W, Lunden B, Vanderpost C (2001). Assessment of vegetation indexes useful for browse (forage) prediction in semi-arid rangelands. Int J Remote Sens, 22(5): 741–756

Mu S J, Chen Y Z, Li J L, Ju W M, Odeh I O A, Zou X L (2013a). Grassland dynamics in response to climate change and human activities in Inner Mongolia, China between 1985 and 2009. Rangeland J, 35(3): 315–329

Mu S J, Li J L, Zhou W, Yang H F, Zhang C B, Ju W M (2013c). Spatial-temporal distribution of net primary productivity and its relationship with climate factors in Inner Mongolia from 2001 to 2010. Acta Ecol Sin, 33(12): 3752–3764 (in Chinese)

Mu S J, Zhou S X, Chen Y Z, Li J L, Ju W M, Odeh I O A (2013b). Assessing the impact of restoration-induced land conversion and management alternatives on net primary productivity in Inner Mongolian grassland, China. Global Planet Change, 108(3): 29–41

Nemani R R, Keeling C D, Hashimoto H, Jolly W M, Piper S C, Tucker C J, Myneni R B, Running S W (2003). Climate-driven increases in global terrestrial net primary production from 1982 to 1999. Science, 300(5625): 1560–1563

Niklaus M, Eisfelder C, Tum M, Günther K P (2012). A remote sensing model based land degradation index for the arid and semi-arid regions of southern Africa. IEEE International Geoscience and Remote Sensing Symposium, IGARSS 2012. 22e27 July 2012, Munich, Germany

Parton W J, Scurlock J M O, Ojıma D S, Gilmanov T G, Scholes R J, Schimel D S, Kirchner T, Menaut J C, Seastedt T, Garcia Moya E, Kamnalrut A, Kinyamario J I (1993). Observations and modeling of biomass and soil organic matter dynamics for the grassland biome worldwide. Global Biogeochem Cycles, 7(4): 785–809

Pei F S, Li X, Liu X P, Lao C H (2013). Assessing the impacts of droughts on net primary productivity in China. J Environ Manage, 114(2): 362–371

Piao S L, Ciais P, Huang Y, Shen Z H, Peng S S, Li J S, Zhou L P, Liu H Y, Ma Y C, Ding Y H, Friedlingstein P, Liu C Z, Tan K, Yu Y Q, Zhang T Y, Fang J Y (2010). The impacts of climate change on water resources and agricultural in China. Nature, 467(7311): 43–51

Piao S L, Fang J Y, Ciais P, Peylin P, Huang Y, Sitch S, Wang T (2009). The carbon balance of terrestrial ecosystems in China. Nature, 458 (7241): 1009–1013

Piao S L, Fang J Y, He J S (2006). Variations in vegetation net primary production in the Qinghai-Xizang plateau, China, from 1982 to 1999. Clim Change, 74(1–3): 253–267

Piao S L, Fang J Y, Zhou L M, Zhu B, Tan K, Tao S (2005). Changes in vegetation net primary productivity from 1982 to 1999 in China. Global Biogeochem Cycles, 19(2): 1605–1622

Potter C, Klooster S, Myneni R, Genovese V, Tan P N, Kumar V (2003). Continental-scale comparisons of terrestrial carbon sinks estimated from satellitedata and ecosystem modeling 1982–1998. Global Planet Change, 39(3–4): 201–213

Potter C, Klooster S, Steinbach M, Tan P N, Kumar V, Shekhar S, Carvalho C R D (2004). Understanding global teleconnections of climate to regional model estimates of Amazon ecosystem carbon fluxes. Glob Change Biol, 10(5): 693–703

Potter C S, Randerson J T, Field C B, Matson P A, Vitousek P A, Mooney H A, Klooster S A (1993). Terrestrial ecosystem production: a process model based on global satellite and surface data. Global Biogeochem Cycles, 7(4): 811–841

Prescott J A (1940). Evaporation from a water surface in relation to solar radiation. Trans R Soc S Aust, 64: 114–125

Prince S D (1991). A model of regional primary production for use with coarse resolution satellite data. Int J Remote Sens, 12(6): 1313–1330

Prince S D, Goward S N (1995). Global primary production: a remote sensing approach. J Biogeogr, 22(4/5): 815–835

Rayner P J, Scholze M, Knorr W, Kaminski T, Giering R, Widmann H (2005). Two decades of terrestrial carbon fluxes from a carbon cycle data assimilation system (CCDAS). Global Biogeochem Cycles, 19 (2): 202–214

Reeves M C, Moreno A L, Bagne K E, Running S W (2014). Estimating climate change effects on net primary production of rangelands in the United States. Clim Change, 126(3–4): 429–442

Ren Z Y, Liu Y X (2013). Contrast in vegetation net primary productivity estimation models and ecological effect value evaluation in Northwest China. Chin. J Eco-Agric, 21(4): 494–502 (in Chinese)

Ruimy A, Dedieu G, Saugier B (1996). TURC: a diagnostic model of continental gross primary productivity and net primary productivity. Global Biogeochem Cycles, 10(2): 269–285

Running S W, Nemani R R, Heinsch F A, Zhao M S, Reeves M, Hashimoto H (2004). A continuous satellite-derived measure of global terrestrial primary production. Bioscience, 54(6): 547–560

Running S W, Thornton P E, Nemani R, Glassy J M (2000). Global terrestrial gross and net primary productivity from the earth observing system. In: Sala O E, Jackson R B, Mooney H A, Howarth R W, eds. Methods in Ecosystem Science. New York: Springer, 44–57

Sellers P J, Randall D A, Collatz G J, Berry J A, Field C B, Dazlich D A, Zhang C, Collelo G D, Bounoua L (1996). A revised land surface parameterization (SiB2) for atmospheric GCMs. Part 1: model formulation. J Clim, 9(4): 676–705

Silvestri S, Marani M, Settle J, Benvenuto F, Marani A (2002). Salt marsh vegetation radiometry: data analysis and scaling. Remote Sens Environ, 80(3): 473–482

Stow D A V, Petersen A, Hope A, Engstrom R, Coulter L L (2007). Greenness trends of Arctic tundra vegetation in the 1990s: Comparison of two NDVI datasets from NOAA AVHRR system. Int J Remote Sens, 28(21): 4807–4822

Sun Q L, Feng X F, Liu M X, Xiao X (2015). Estimation and analysis of net primary productivity in Wuling mountainous area based on remote sensing. Journal of Natural Resources, 347: 83–95 (in Chinese)

Tang C J, Fu X Y, Jiang D, Fu J Y, Zhang X Y, Zhou S (2014). Simulating spatiotemporal dynamics of Sichuan grassland net primary productivity using the CASA model and in situ observations. Sci World J, 2014: 956963

UN (1994). Elaboration of an International Convention to Combat Desertification in Countries Experiencing Serious Drought and/or Desertification, Particularly in Africa. UN General Assembly. A/AC.241/27. Available online at: http://www.unccd.int/convention/text/pdf/conv-eng.pdf (accessed 17.03.10)

Verstraete M M (1986). Defining desertification: a review. Clim Change, 9(1–2): 5–18

Wang H, Li X B, Long H L, Gai Y Q, Wei D D (2009). Monitoring the effects of land use and cover changes on net primary production: a case study in China's Yongding River basin. For Ecol Manage, 258 (12): 2654–2665

Wang P J, Xie D H, Zhou Y Y, E Y H, Zhu Q J (2014). Estimation of net primary productivity using a process-based model in Gansu Province, Northwest China. Environ Earth Sci, 71(2): 647–658

Wang X C, Wang S D, Zhang H B (2013). Spatiotemporal pattern of vegetation net primary productivity in Henan Province of China based on MOD17A3. Chinese J Ecol, 32(10): 2797–2805 (in Chinese)

Woodward F I, Smith T M, Emanuel W R (1995). A global land primary productivity and phytogeography model. Global Biogeochem Cycles, 9(4): 471–490

Xie B N, Qin Z F, Wang Y, Chang Q R (2014). Spatial and temporal variation in terrestrial net primary productivity on Chinese Loess Plateau and its influential factors. Transactions of the Chinese Society of Agricultural Engineering, 30(11): 244–253 (in Chinese)

Xu J H (2010). Geographic Modeling Method. Beijing: Science Press (in Chinese)

Yu D Y, Shao H B, Shi P J, Zhu W Q, Pan Y Z (2009). How does the conversion of land cover to urban use affect net primary productivity? A case study in Shenzhen city, China. Agric Meteorol, 149(11): 2054–2060

Yu D Y, Shi P J, Han G Y, Zhu W Q, Du S Q, Xun B (2011). Forest ecosystem restoration due to a national conservation plan in China. Ecol Eng, 37(9): 1387–1397

Zhao G S, Wang J B, Fan W Y, Ying T Y (2011). Vegetation net primary productivity in Northeast China in 2000–2008: simulation and seasonal change. Chinese J Appl Ecol, 22(3): 621–630 (in Chinese)

Zhao S Q (1983). A new scheme for comprehensive physical regionalization in China. Acta Geogr Sin, 38(1): 1–10 (in Chinese)

Zheng S H, Zhao M L, Shan D, Pan L R, Han G D (2005). Range condition and its evaluation. Grassland of China, 27(2): 72–76 (in Chinese)

Zhou W, Gang C C, Zhou L, Chen Y Z, Li J L, Ju W M, Odeh I (2014). Dynamic of grassland vegetation degradation and its quantitative assessment in the northwest China. Acta Oecol, 55(2): 86–96

Zhu W Q, Pan Y Z, Long Z H, Chen Y H, Li J, Hu H B (2005). Estimating net primary productivity of terrestrial vegetation based on GIS and RS: a case study in Inner Mongolia, China. J Remote Sens, 9 (3): 300–307 (in Chinese)